
GRAPH STRUCTURAL RESIDUALS: A LEARNING APPROACH TO DIAGNOSIS

Jan Lukas Augustin

Institute of Automation Technology
Helmut Schmidt University, Hamburg, Germany
janlukas.augustin@hsu-hh.de

Oliver Niggemann

Institute of Automation Technology
Helmut Schmidt University, Hamburg, Germany
oliver.niggemann@hsu-hh.de

ABSTRACT

Traditional model-based diagnosis relies on constructing explicit system models, a process that can be laborious and expertise-demanding. In this paper, we propose a novel framework that combines concepts of model-based diagnosis with deep graph structure learning. This data-driven approach leverages data to learn the system's underlying structure and provide dynamic observations, represented by two distinct graph adjacency matrices. Our work facilitates a seamless integration of graph structure learning with model-based diagnosis by making three main contributions: redefining the constructs of system representation, observations, and faults; introducing two distinct versions of a self-supervised graph structure learning model architecture; and demonstrating the potential of our data-driven diagnostic method through experiments on a system of coupled oscillators.

1 Introduction

Diagnosing faults in complex systems has become a cornerstone challenge in artificial intelligence and engineering. Historically, model-based diagnosis (MBD) has been the primary methodology, with two main lines of research championing distinct approaches. Consistency-based diagnosis, deeply rooted in the realms of logic and optimization, offers a structured approach emphasizing system representation, observations, and health states. In contrast, the fault detection and isolation (FDI) community, grounded in engineering and control theory disciplines, leans towards continuous models that dynamically represent the states of systems. While undeniably robust and powerful, these approaches come with a clear challenge: the manual construction of system models, which is not only effort-intensive but also demands specialized expertise.

Parallel to the challenges faced in the traditional MBD arena, deep learning has emerged as a transformative force in learning complex representations directly from data. While Convolutional Neural Networks (CNNs) and Long Short-Term Memory networks (LSTMs) have redefined time-series data analysis, Graph Neural Networks (GNNs) have shown unparalleled aptitude in learning from structured data. Notably, GNNs have demonstrated exceptional performance in static datasets such as citation networks, but their potential in dynamic systems like CPS remains under-explored.

Our work bridges this divide. Building upon our prior insights and driven by the need for more flexible and adaptive diagnostic tools, we introduce a novel, learning-centric approach to model-based diagnosis that integrates deep graph structure learning with traditional diagnostic paradigms. At the heart of our approach is the representation of systems as spatiotemporal graphs. We present two novel models: a reference model that discerns a static representation of a system's normative behavior, and an observation model that produces dynamic graph structures based on current inputs. The primary novelty lies in identifying faults as discrepancies between these learned graph structures, marking a paradigm shift from traditional component health state assessments to the identification of faulty edges.

Our goal revolves around a pivotal question: can we redefine the principles of system representation, observations, and faults in the context of graph structural learning, and leverage this redefinition to craft a data-driven diagnostic mechanism? Pursuant to this, our research revolves around the following queries:

1. Can we learn a system’s inherent structure, represented as the adjacency matrix of a graph, purely from observational data?
2. Is it feasible to construct a model that dynamically crafts observations, encapsulated as adjacency matrices, contingent on windows of multivariate time-series inputs?
3. Can the discrepancies between a learned static structure and dynamic observations serve as a basis to detect faults?

Reflecting on these research questions, we make the ensuing contributions:

1. We present a novel redefinition of system representation, observations, and faults, enabling an elegant confluence of graph structure learning with the tenets of MBD. This foundational perspective drives our data-driven diagnostic approach.
2. We elucidate two distinctive graph structure learning models in a self-supervised way. One is trained to provide a static reference adjacency matrix encapsulating a normative system representation, while the other dynamically generates observation adjacencies based on current system inputs.
3. Through empirical analyses on a dataset of coupled oscillators, we showcase the efficacy of our diagnostic method.

In doing so, we aim to harmonize model-based diagnosis and deep learning, using the strengths of both to enhance the diagnostic capabilities. Our method **Graph Structural Residuals (GSR)** seeks to contribute to the research field by providing an innovative, data-driven approach to diagnosis. By learning directly from data, we expect to alleviate the need for manual model creation, paving the way for more automated and scalable diagnostic systems.

2 Related Work

Model-based diagnosis research is an active field that has attracted interest from various disciplines, leading to multiple distinct research tracks. Notably, consistency-based diagnosis and fault detection and isolation can both be regarded as prominent tracks of MBD [1]. Despite their common interest in diagnosing systems, they have evolved independently, originating from different foundational backgrounds.

Consistency-based diagnosis is rooted in the fields of logic, combinatorial optimization, search, and complexity analyses. The focus lies in finding minimal sets of components that, when assumed faulty, make the system’s behavior consistent with the observations [2, 3]. MBD has been studied in numerous domains including automotive [4], space [5], robotics [6], software [7] and cyber-physical systems [8]. Classic approaches include GDE [2], CDA* [9] or SDE [10]. Components play an instrumental role in this model; their behavior, and the interplay among them, forms the cornerstone of diagnostic inferences.

On the other hand, the **fault detection and isolation** is deeply rooted in engineering disciplines, particularly control theory and statistical decision-making [11, 2]. An essential tool in FDI is the generation and use of residuals, which are computed as the difference between measured and expected system behaviors [12]. Structural analysis is a prevalent approach in FDI, providing insights into system behaviors based on the interconnections between system components without necessarily diving into detailed quantitative models [13, 14]. It allows to check the diagnosability of a system and ensure optimal sensor placement [15].

While traditional MBD emphasizes system models and relations of components, another emergent field seeks to harness the structure inherent in data itself: the realm of **graph neural networks (GNNs)** [16] in which graphs serve as powerful data representation structures in various domains, ranging from social networks to molecular architectures. To capture the intricate relationships within graph-structured data, Graph Neural Networks (GNNs) have emerged as the forefront technology [17]. GNNs operate on the principle that a node’s state is influenced by its neighbors, effectively modeling complex graph patterns [18, 19]. One notable variant, Graph Convolution Networks (GCNs), aggregate the representations of a node’s immediate neighbors to form its feature representation [20, 21]. Such techniques have paved the way for breakthroughs in diverse applications, from traffic prediction [22, 23] and recommendation systems [24] to multi-relational data tasks [25].

While GNNs have exhibited robust performance on predefined graph structures, there exists an intriguing avenue of research focused on learning or refining the graph structure from data. Termed as **graph structure learning (GSL)**, this paradigm addresses scenarios where the graph topology is either not provided a priori or can be optimized using available data [26]. GSL strategies typically revolve around adjustable adjacency matrices, representing adjacency with learnable parameters, and optimizing it in conjunction with GNNs for tasks like node classification [27, 28, 29, 30, 31].

While deep GSL approaches have shown promise, they often depend on a supervised scenario. In the absence of labels we use a self-supervised approach inspired by SLAPS [32].

3 Preliminaries and Notation

In this section, we lay the foundational concepts required to understand our approach, along with the accompanying notation. Our work takes a graph-centric view on fault diagnosis by considering both the normative system representation and the observation to be outputs of learnable deep learning models. Consequently, faults are calculated as deviations between reference and observation graphs.

3.1 Architecture

While various graph structure learning algorithm may be used to generate the necessary adjacency matrices, in the absence of labels we suggest a self-supervised approach. As shown in Figure 1, the two-stage model architecture consists of a graph generator module and a denoising module, which are trained end-to-end to minimize the reconstruction error. The reconstruction error serves as an indirect supervision signal to guide the graph generator to output weighted edges that resemble the connections of the underlying structure from which the data has been generated.

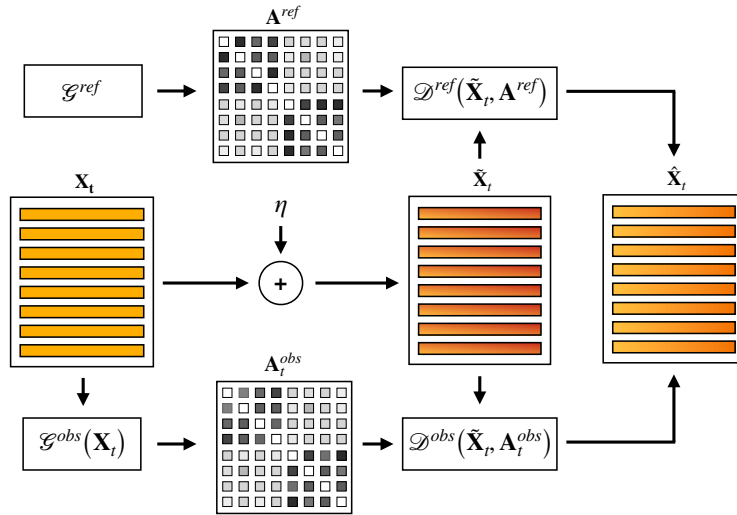


Figure 1: Overview of the GSR architecture during training. Given a noisy version $\tilde{\mathbf{X}}_t$ of input features \mathbf{X}_t that are generated from a system with an unknown underlying structure, denoising modules \mathcal{D}^{ref} and \mathcal{D}^{obs} are trained to reconstruct the original features using adjacencies \mathbf{A}^{ref} and \mathbf{A}_t^{obs} generated by graph generators \mathcal{G}^{ref} or \mathcal{G}^{obs} , respectively.

3.2 Multivariate time series

A multivariate time series is a collection of observations from multiple variables recorded over the same time intervals. Such data is often represented as a matrix, where each row corresponds to a variable and each column represents a time step. Given:

- T : Length of the multivariate time series.
- N : Number of variables (equals number of nodes $|V|$ in the graph) - these can be inputs, outputs, or measurements.
- W : Length of the time window.
- η : Artificially generated noise.

Definition 1 (Multivariate Time Series Window).

A window of multivariate time series data starting at time t and ending at time $t + W$ is represented by the matrix

$\mathbf{X}_{t:t+W}$ where $\mathbf{X}_{t:t+W} \in \mathbb{R}^{N \times W}$. If $\eta_{t:t+W}$ denotes noise in this window, an intentionally corrupted version is given by:

$$\tilde{\mathbf{X}}_{t:t+W} = \mathbf{X}_{t:t+W} + \eta_{t:t+W}$$

To preserve readability in the text, we also refer to $\mathbf{X}_{t:t+W}$ as \mathbf{X}_t .

3.3 Spatiotemporal graphs

Spatiotemporal graphs introduce a temporal dimension into classical graph structures, enabling the representation of interactions and relationships that evolve over time [33]. We take a discrete temporal snapshot view by considering time windows and introduce two types of graphs: Static spatiotemporal graphs that do not evolve over time are used to obtain the reference structure and dynamic spatiotemporal graphs that depend on the temporal signal provide the observation structure. Given:

- G : A graph where nodes V represent variables and adjacency matrix \mathbf{A} depicts their relationships.
- \mathbf{A} : Adjacency matrix of graph G where $\mathbf{A} \in \mathbb{R}^{N \times N}$.
- $\mathbf{X}_{t:t+W}$: A multivariate time series for given time window.

Definition 2.1 (Static Spatiotemporal Graph).

Let $G = \{V, \mathbf{A}, \mathbf{X}_{t:t+W}\}$ be a spatiotemporal graph where the strength and direction of relationships are quantified by its adjacency matrix \mathbf{A} , and each element A^{ij} represents the weight of the edge between node i and node j .

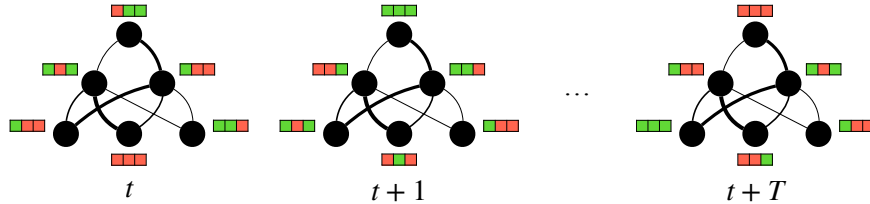


Figure 2: Static spatiotemporal graph with static \mathbf{A}

Definition 2.2 (Dynamic Spatiotemporal Graph).

Let $G = \{V, \mathbf{A}_t, \mathbf{X}_{t:t+W}\}$ be a spatiotemporal graph where the strength and direction of relationships are quantified by its time-dependent adjacency matrix \mathbf{A}_t , and each element A_t^{ij} represents the weight of the edge between node i and node j for a time window starting at time t and ending at time $t + W$.

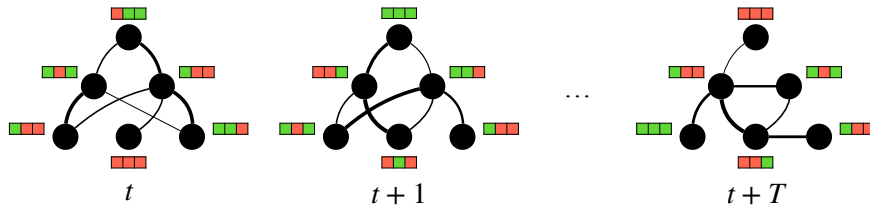


Figure 3: Dynamic spatiotemporal graph with time-dependent \mathbf{A}_t

3.4 Graph Generator Module

The graph generator module is designed to be trained to generate the adjacency matrix that serves as an input of the denoising module. The generation happens depending on learnable parameters and - in the case of the observation graph generator - the multivariate time series. Given:

- $\mathcal{G}(\cdot)$: Graph generator function.
- θ_G : Learnable parameters of the graph generator function.

Definition 3 (Graph Generator Module).

For a time series data window $\mathbf{X}_{t:t+W}$, the adjacency matrices \mathbf{A}^{ref} and \mathbf{A}_t^{obs} are outputted by the reference and observation graph generator modules, respectively. They are defined as:

$$\mathbf{A}^{ref} = \mathcal{G}^{ref}(\theta_{\mathcal{G}^{ref}}) \quad (1)$$

$$\mathbf{A}_t^{obs} = \mathcal{G}^{obs}(\mathbf{X}_{t:t+W}, \theta_{\mathcal{G}^{obs}}) \quad (2)$$

For better readability in the text, we also refer to \mathbf{A}^{ref} and \mathbf{A}_t^{obs} as \mathbf{A} if the information given is independent of the module used.

3.5 Denoising Module

The denoising module is built to be trained to eliminate or reduce the noise and reconstruct the original multivariate time series data given a noisy version of it and the adjacency matrix provided by the graph generator module. Given:

- $\mathcal{D}(\cdot, \cdot)$: Denoising function.
- $\theta_{\mathcal{D}}$: Parameters of the denoising function.

Definition 4 (Denoising Module).

For a noisy time series data window $\tilde{\mathbf{X}}_{t:t+W}$, the denoised versions using the reference and observation models, $\hat{\mathbf{X}}_{t:t+W}^{ref}$ and $\hat{\mathbf{X}}_{t:t+W}^{obs}$, are calculated by \mathcal{D} as follows:

$$\hat{\mathbf{X}}_{t:t+W}^{ref} = \mathcal{D}^{ref}(\tilde{\mathbf{X}}_{t:t+W}, \mathbf{A}^{ref}, \theta_{\mathcal{G}^{ref}}) \quad (3)$$

$$\hat{\mathbf{X}}_{t:t+W}^{obs} = \mathcal{D}^{obs}(\tilde{\mathbf{X}}_{t:t+W}, \mathbf{A}_t^{obs}, \theta_{\mathcal{G}^{obs}}) \quad (4)$$

3.6 Graph Structural Residuals

In systems characterized by graph structures, understanding the deviation or residual between the observed and reference relationships is pivotal. The residuals can provide insights into discrepancies, misalignments, or faults in the system. For the context of this work, we define a residual function that can be used after the model has been trained (see Figure 4). It maps the reference and observation adjacency matrices to a residual matrix highlighting these deviations.

Given:

- \mathbf{A}^{ref} : Reference adjacency matrix obtained from the trained reference graph generator module.
- \mathbf{A}_t^{obs} : Time-dependent observed adjacency matrix for a specific time window obtained from the trained observation graph generator module.

Definition 5 (Graph Structural Residual).

The residual matrix, \mathbf{R}_t , for a given time window starting at time t is a function of the difference between the reference and observed adjacency matrices. It can be defined using the function $\mathcal{R}(\cdot, \cdot)$ as:

$$\mathbf{R}_t = \mathcal{R}(\mathbf{A}^{ref}, \mathbf{A}_t^{obs}) \quad (5)$$

For the simplest case, the residual function \mathcal{R} computes the absolute value of the difference between the reference and observed adjacency matrices. If a threshold τ is defined, all entries in \mathbf{R}_t that are below τ can be set to zero, denoting them as insignificant residuals. In essence, each entry R_t^{ij} in \mathbf{R}_t quantifies the deviation of the edge weight between node i and node j from the reference to the observed structure for the time window starting at t .

$$\mathbf{R}_t = \begin{cases} |\mathbf{A}^{ref} - \mathbf{A}_t^{obs}| & \text{if } |\mathbf{A}^{ref} - \mathbf{A}_t^{obs}| \geq \tau \\ 0 & \text{otherwise} \end{cases} \quad (6)$$

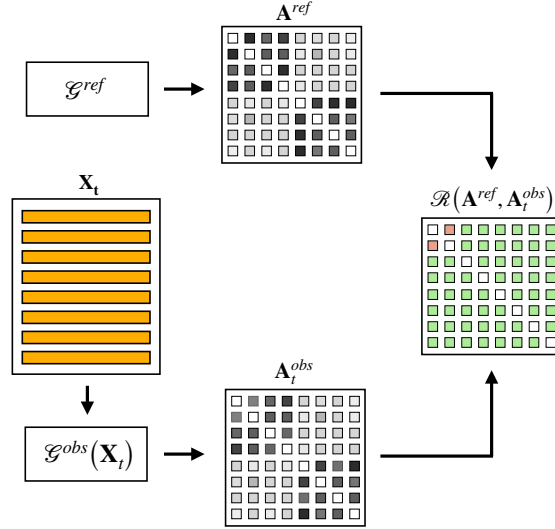


Figure 4: Overview of the GSR architecture generating residuals. Given input features X adjacencies A^{ref} and A_t^{obs} generated by graph generators \mathcal{G}^{ref} or \mathcal{G}^{obs} , respectively. Graph structural residuals R_t are calculated as deviations between reference and observation to detect faulty edges.

3.7 Diagnosis

In traditional model-based diagnosis, diagnosis is defined as the process of identifying the components or parts of the system that are malfunctioning, often based on a discrepancy between observed behavior and a reference or expected behavior. However, our graph-centric approach shifts the focus from identifying faulty components to identifying faulty edges or relationships between nodes. This is because the behavior of interconnected systems can be strongly influenced by the relationships between system variables rather than the variables themselves.

Given:

- R_t : Residual matrix for a given time window starting at time t , as defined in Section 3.6.
- δ : A diagnosis threshold that determines the significance of an edge fault.

Definition 6 (Edge-based Diagnosis).

A diagnosis D_t for a given time window starting at time t is a binary matrix of the same dimensions as R_t where each element D_t^{ij} is determined as:

$$D_t^{ij} = \begin{cases} 1 & \text{if } R_t^{ij} \geq \delta \\ 0 & \text{otherwise} \end{cases} \quad (7)$$

Here, a value of 1 in D_t represents a faulty edge between nodes i and j , while a value of 0 indicates the edge is considered non-faulty for the given time window. The diagnosis D_t serves as an interpretable map highlighting the regions in the graph structure that deviate significantly from the expected norm, thus enabling targeted investigations and corrective actions.

4 Methodology

In the realms of fault diagnosis, CBD and FDI start out with manual modeling processes to represent system dynamics and behavior, allowing them to detect deviations and infer potential faults. In contrast, our proposed methodology hinges on leveraging learning-based mechanisms to capture relations which can be later employed for fault diagnosis. Conceptually, our methodology can be discerned into two core stages, akin to CBD and FDI, albeit with stark distinctions in the means of achieving the desired outcomes:

Model Construction: Unlike traditional methods where this stage is manual, we employ a learning-based approach. Our model is trained to identify underlying system behaviors, relationships, and dynamics.

Fault Diagnosis: Post the construction (or training) of the model, we use it for generating graph structural residuals. These residuals, as previously introduced, provide insights into the discrepancies between the expected and observed system behaviors, thereby allowing us to pinpoint potential faults.

With this overarching view in mind, we delve deeper into the nuances of both stages in the following subsections.

4.1 Model Construction

By choosing a GNN for our denoising autoencoder module we make use of the smoothness assumption GNNs are built upon, which posits that connected nodes in a graph are likely to have similar features or labels [34]. The graph generator is incentivized to provide a graph with high homophily since the GNN requires information to come from relevant neighboring nodes to reconstruct the original features in the best possible way.

Given that inputs consist of time series data, we incorporate an additional inductive bias to guide the learning process by applying Temporal Convolutional Networks (TCNs) [35] in both the observation graph generator and the denoising autoencoder module. TCN ensures the model respects the causal structure of the time series data by using causal convolutions, makes nearby time steps more relevant than distant ones, utilizes dilated convolutions to increase the model’s receptive field and includes residual connections to facilitate the flow of gradients.

4.1.1 Graph Generator Modules

Both generators implement a function \mathcal{G} with parameters $\theta_{\mathcal{G}}$ which produces a matrix \mathbf{A} as output. We apply an activation function to a preliminary adjacency $\tilde{\mathbf{A}}$ before symmetrizing and normalizing it to obtain the adjacency matrix \mathbf{A} which is subsequently used by the GNN layers of the denoising module \mathcal{D} . For the reference graph generator we apply the exponential linear unit (ELU) to avoid gradient flow problems in case any edge becomes negative and for the observation graph generator we apply the sigmoid function. Note that while we could also generate directed graphs, i.e. non-symmetric adjacency matrices, in our experiments we decide to restrict our model to undirected graphs to stabilize training. We consider the following two graph generators:

During training the **reference graph generator** \mathcal{G}^{ref} directly optimizes the adjacency matrix fully parametrized by $\theta_{\mathcal{G}^{ref}}$ while ignoring the input node features. Consequently, the generator provides a single static matrix \mathbf{A}^{ref} that is optimized on all samples of the training set and represents the structure of the system during normal operation.

For the **observation graph generator** \mathcal{G}^{obs} the parameters $\theta_{\mathcal{G}^{obs}}$ correspond to the weights of a TCN and $\tilde{\mathbf{A}} = \mathcal{G}^{obs}(\mathbf{X}, \theta_{\mathcal{G}^{obs}}) = \text{TCN}(\mathbf{X}_t) \cdot \text{TCN}(\mathbf{X}_t)^T = \mathbf{X}'_t \cdot \mathbf{X}'_t{}^T$, where the function $\text{TCN} : \mathbb{R}^{N \times W} \rightarrow \mathbb{R}^{N \times W}$ produces a matrix with updated node representations \mathbf{X}'_t . Dot product is applied as a similarity measure that maps $\mathbb{R}^{N \times W} \rightarrow \mathbb{R}^{N \times N}$. Note that TCN is applied to each univariate time series separately making \mathcal{G}^{obs} permutation equivariant.

4.1.2 Denoising Modules

The task of the denoising module \mathcal{D} is to take a noisy version $\tilde{\mathbf{X}}_t$ of the node features \mathbf{X}_t and the generated adjacency matrix \mathbf{A} as inputs and produce the updated denoised node features $\hat{\mathbf{X}}_t$ as output. We add independent Gaussian noise η_t to \mathbf{X}_t to obtain $\tilde{\mathbf{X}}_t = \mathbf{X}_t + \mathcal{N}(\mu, \sigma^2)^{N \times W}$. We use the same GNN-based implementation for both the reference and the observation denoising modules. In the following we introduce our graph TCN layers.

4.1.3 Graph TCN Layers

GNNs use the graph structure and node features \mathbf{x}_i to learn a representation vector of a node, \mathbf{h}_i . Representation of nodes are iteratively updated by aggregating representations of their neighbors. Following the notation of the Graph Isomorphism Network (GIN) [36], after k iterations of aggregation, a node’s representation captures information from its k -hop network neighborhood. Formally, the k -th layer of a GNN is

$$a_i^{(k)} = \text{AGGREGATE}^{(k)} \left(\left\{ h_j^{(k-1)} : u \in \mathcal{N}(v) \right\} \right), \tag{8}$$

$$h_i^{(k)} = \text{COMBINE}^{(k)} \left(h_i^{(k-1)}, a_i^{(k)} \right), \tag{9}$$

where $\mathbf{h}_i^{(k)}$ is the feature vector of node i at the k -th iteration/layer. In the first layer $\mathbf{h}_i^{(0)} = \mathbf{x}_i$, and $\mathcal{N}(i)$ is a set of nodes adjacent to node i .

We design a custom graph layer with similarities to the popular GIN layers [36] (Equation 10).

$$h_i^{(k)} = \text{MLP}^{(k)} \left(\left(1 + \epsilon^{(k)} \right) \cdot h_i^{(k-1)} + \sum_{j \in \mathcal{N}(i)} h_j^{(k-1)} \right) \quad (10)$$

However, connections are weighted, we use a TCN instead of an MLP and only apply it to the representations of neighboring nodes, excluding self-loops. We use residual connections for all layers except the output layer to allow for a deeper network while also forcing the GNN to use \mathbf{A} . Note that TCN parameters are shared within a layer, i.e. the same TCN is applied to each aggregated node representation of that layer. Hence, the AGGREGATE step in Equation 8 becomes a weighted sum

$$a_v^{(k)} = \sum_j \mathbf{A}_{ij} \cdot \mathbf{h}_j^{(k-1)} \quad (11)$$

and the COMBINE step from Equation 9 for a graph TCN layer reads as

$$h_i^{(k)} = \mathbf{h}_i^{(k-1)} + \sigma \left(\text{TCN} \left(a_v^{(k)} \right) \right) \quad (12)$$

so that the entire layer can be described by

$$\mathbf{h}_i^{(k)} = \mathbf{h}_i^{(k-1)} + \sigma \left(\text{TCN} \left(\sum_{j \in \mathcal{N}(i)} \mathbf{A}_{ij} \cdot \mathbf{h}_j^{(k-1)} \right) \right). \quad (13)$$

For our use case the node representations are noisy features so that $\mathbf{h}_i^{(k)} = \tilde{\mathbf{x}}_t^{(k)}$. Rewritten in matrix form the hidden layers are defined by

$$\tilde{\mathbf{X}}_t^{(k)} = \mathbf{I} \cdot \tilde{\mathbf{X}}_t^{(k-1)} + \sigma \left(\text{TCN} \left(\mathbf{A} \cdot \tilde{\mathbf{X}}_t^{(k-1)} \right) \right), \quad (14)$$

while the output layer without residual connection is defined as

$$\hat{\mathbf{X}}_t^{(k)} = \text{TCN} \left(\mathbf{A} \cdot \tilde{\mathbf{X}}_t^{(k-1)} \right) \quad (15)$$

forcing the model to optimize \mathbf{A} .

4.1.4 Training

As outlined in algorithm 1, during training, for the reference model we minimize the loss function \mathcal{L} , in this case the mean-squared error loss:

$$\mathcal{L} = \text{L}(\mathbf{X}_t, \mathcal{D}^{ref}(\tilde{\mathbf{X}}_t, \mathbf{A}^{ref}, \theta_{\mathcal{D}^{ref}})) \quad (16)$$

where

$$\mathbf{A}^{ref} = \mathcal{G}^{ref}(\theta_{\mathcal{G}^{ref}})$$

and for the observation model we minimize:

$$\mathcal{L} = \text{L}(\mathbf{X}_t, \mathcal{D}^{ref}(\tilde{\mathbf{X}}_t, \mathbf{A}_t^{obs}, \theta_{\mathcal{D}^{obs}})) \quad (17)$$

where

$$\mathbf{A}_t^{obs} = \mathcal{G}^{obs}(\mathbf{X}_t, \theta_{\mathcal{G}^{obs}})$$

4.2 Fault Diagnosis

As outlined in algorithm 2 and following Equation 5, the residual matrix \mathbf{R}_t

Algorithm 1 Training models**Inputs:** Dataset \mathcal{X}_{train} , EPOCHS, BATCH_SIZE**Parameters:** $\theta_{G^{ref}}, \theta_{D^{ref}}, \theta_{G^{obs}}, \theta_{D^{obs}}$ **Output:** Trained modules $G^{ref}, D^{ref}, G^{obs}, D^{obs}$

```

1: Initialize parameters and optimizer
2: for model in {reference, observation} do
3:   for epoch in EPOCHS do
4:     Shuffle  $\mathcal{X}_{train}$ 
5:     for batch in  $\mathcal{X}_{train}$  with size BATCH_SIZE do
6:       Get corrupted version  $\tilde{\mathcal{X}}_{batch}$  adding noise  $\eta$ 
7:       Generate adjacency matrices  $\mathbf{A}$ 
8:       Compute denoised version  $\hat{\mathcal{X}}_{batch}$ 
9:       Compute reconstruction loss
10:      Backpropagate the loss and update parameters
11:    end for
12:  end for
13: end for

```

Algorithm 2 Fault diagnosis using GSR**Inputs:** Dataset $\mathcal{X}_{test}, G^{ref}, D^{ref}, G^{obs}, D^{obs}, \tau$ **Output:** Residual matrix \mathbf{R}_t for all time windows in \mathbf{D}_{test}

```

1: for each time window in  $\mathcal{X}_{test}$  do
2:   Generate  $\mathbf{A}^{ref}$  and  $\mathbf{A}_t^{obs}$ 
3:   Compute the residual matrix  $\mathbf{R}_t$  using  $\mathcal{R}$ 
4:   Filter residuals in  $\mathbf{R}_t$ 
5:   Apply  $\delta$  to obtain binary diagnosis matrix  $\mathbf{D}_t$ 
6: end for

```

5 Experiments

5.1 Dataset

We generate our synthetic dataset using simulations of phase-coupled oscillators[37]. The Kuramoto model is a nonlinear system of phase-coupled oscillators that can exhibit a range of complicated dynamics based on the distribution of the oscillators' internal frequencies and their coupling strengths. We use the common form for the Kuramoto model of n oscillators given by the following differential equation:

$$\frac{d\phi_i}{dt} = \omega_i + \sum_{j \neq i} k_{ij} \sin(\phi_i - \phi_j)$$

with phases ϕ_i , coupling constants k_{ij} , and intrinsic frequencies ω_i . We simulate eight phase-coupled oscillators in 1D with intrinsic frequencies $\omega_i \sim \mathcal{N}(\mu, \sigma)^{n \times d}$ and initial phases $\phi_i^{t=1}$ uniformly sampled from $[0, 2\pi)$. We create two subsystems of connected oscillators by coupling all of the first four as well as all of the last four oscillators.

We connect pairs of oscillators v_i and v_j by setting the corresponding coupling constant $k_{ij} = k_{ji} = k$. All other coupling constants are set to 0. The resulting matrix \mathbf{K} describes the underlying structure of the system of coupled oscillators and can therefore be treated as the ground truth coupling matrix \mathbf{C} when using our proposed method.

5.1.1 Training and Validation

The model is built to denoise multivariate time series with W time steps. We run the simulation for $2W$ time steps so that with each run of the simulation we obtain a signal matrix $\mathbf{S} \in \mathbb{R}^{N \times 2W}$. Samples of the training set \mathcal{X}_{train} comprise the first W time steps whereas the validation set \mathcal{X}_{val} includes the last W time steps of the corresponding simulation runs. See Figure 5 for a visualization of a training sample.

Parameters of the Kuramoto model such as intrinsic frequencies and coupling constants are chosen in such a way that within the first W time steps, depending on the initial phases, the oscillators are generally not yet fully synchronized making the training task non-trivial. In contrast, validation data covers a time span in which the system is already largely synchronized. This makes the reconstruction even more dependent on a correct adjacency matrix \mathbf{A} .

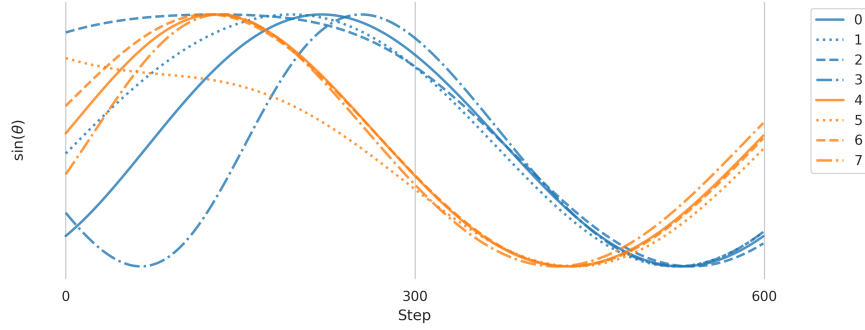


Figure 5: Visualization of a signal S . Nodes 0-3 and nodes 4-7 synchronize due to coupling C shown in Figure 6a.

5.1.2 Diagnosis

Diagnosis data is generated analogously to training and validation data. However, after $2W$ time steps we change the underlying structure by shuffling C to replace it with a perturbed coupling matrix \hat{C} . The simulation continues for another $3W$ steps and the system starts to synchronize and reach a new stable state. These last $3W$ steps are considered for diagnosis.

5.2 Experimental Setup

We train two models as outlined in Algorithm 1. Baseline configurations include:

- **True**, which assumes that the underlying structure is known. $A^{true} = C$ replaces the output of the graph generator,
- **Correlations**, which replaces the output of the graph generator with A^{corr} , a correlation matrix calculated by averaging the Pearson correlation over all samples of the training set, and
- **Features**, which ignores the TCN in the dynamic observation graph generator to calculate similarity between nodes directly from the untransformed features.

5.2.1 Adjacency error metric

We are interested in the agreement between the ground truth coupling matrix C and the inferred adjacency matrix A . Since self-loops are ruled out in order to force denoising module \mathcal{D} to make use of informative nodes, entries of the matrix diagonals are masked out and hence also not considered for the evaluation of A . To adjust for differences in scale, A is rescaled to range $[0, 1]$ before calculating the adjacency error, $e_{adj} = MAE(A, C)$ which indicates whether the model is learning the correct structure.

5.2.2 Reconstruction error metric

Even though minimizing the reconstruction error is merely used as a means for the model to learn the structure of the underlying system, it is still a metric worth tracking since it could be used to perform anomaly detection and trigger the diagnosis. Same as for the loss, the reconstruction error e_{rec} is calculated as the mean squared error between the input signal X and the denoised output \hat{X} , $e_{rec} = MSE(\hat{X}, X)$.

5.2.3 Implementation details

We implemented our model in PyTorch [38] and used the Kuramoto package [39] to run simulations utilizing five different seeds to account for randomness. We trained the model for 50 epochs using the Adam [40] optimizer with a learning rate of 0.001, and a batch size of 16. We identified suitable hyperparameters [layers: 2, dropout: 0.5] for the denoising autoencoder based on the reconstruction error on the validation set. For the TCN proven parameters were chosen based on the original publication [35]. We ran all experiments on a n1-standard-8 instance with 8 vCPUs, 30 GB of memory and a single Tesla T4 GPU.

Table 1: Validation results given as mean \pm standard deviation for five different seeds.

Goal	Configuration	e_{adj}	e_{rec}
ref	True	0.000 \pm 0.000	0.138 \pm 0.067
ref	\mathcal{G}^{ref}	0.050 \pm 0.018	0.144 \pm 0.058
ref	Correlation	0.119 \pm 0.027	0.139 \pm 0.057
obs	\mathcal{G}^{obs}	0.260 \pm 0.009	0.117 \pm 0.014
obs	Features	0.457 \pm 0.002	0.240 \pm 0.034

5.3 Results

5.3.1 Learning the Reference Model

Validation results given in Table 1 show that the \mathcal{G}^{ref} generator improves upon the Correlation baseline in terms of adjacency error and yields results comparable to True and Correlation baselines with respect to reconstruction error.

Figure 6b shows the reference adjacency \mathbf{A}^{ref} generated by \mathcal{G}^{ref} alongside the ground truth \mathbf{C} . \mathbf{A}^{ref} represents the average relations of nodes over all samples. Randomness introduced via different initial conditions of individual samples is reflected by variations in \mathbf{A}^{ref} but \mathbf{C} can be recovered by applying a threshold.

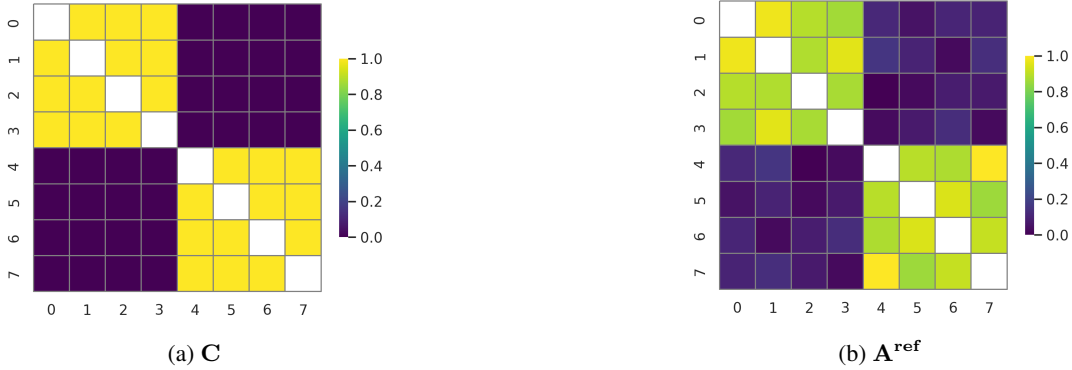


Figure 6: Comparison of (a) the coupling matrix \mathbf{C} defining the underlying structure and (b) the reference adjacency \mathbf{A}^{ref} generated by \mathcal{G}^{ref} .

5.3.2 Learning the Observation Model

Validation results given in Table 1 show that the observation graph generator \mathcal{G}^{obs} improves upon the Features baseline both in terms of adjacency error as well as with respect to reconstruction error. Note that when comparing to \mathcal{G}^{ref} we see that \mathcal{G}^{obs} shows the best results with respect to reconstruction error but poorer adjacency error. This is expected since \mathcal{G}^{ref} learns a set of parameters that best describe the system on average, while the dynamic \mathcal{G}^{obs} can and will adjust the adjacency to the inputs. This behavior is illustrated in Figure 7 which shows two observation adjacency matrices \mathbf{A}^{obs} for two different input samples.

5.3.3 Obtaining Graph Structural Residuals

For robustness, we calculate the mean over a set of time windows $\mathcal{W} = w_1, w_2, \dots, w_m$, where m is the number of windows. Each window w_i is defined by the start step s_i and fixed length T . Given that the observation adjacency matrix for each time window w_i is $\mathbf{A}_i^{obs}(\mathbf{X}_i)$, the average observation adjacency matrix $\mathbf{A}_{avg}^{obs}(\mathcal{W})$ over the set of time windows can be calculated as:

$$\mathbf{A}_{avg}^{obs}(\mathcal{W}) = \frac{1}{m} \sum_{i=1}^m \mathbf{A}_i^{obs}(\mathbf{X}_i) \quad (18)$$

We can then calculate the residual matrix \mathbf{R}_t for a set of time windows analogously to Equation 5:

$$\mathbf{R}_t(\mathcal{W}) = |\mathbf{A}^{ref} - \mathbf{A}_{avg}^{obs}(\mathcal{W})|$$



Figure 7: Examples of observation adjacency matrices \mathbf{A}^{obs} generated by \mathcal{G}^{obs} for two validation samples.

5.3.4 Case 1 - Decoupling

For our first test case we consider a system in which a component is decoupled from its neighbors. We adjust \mathbf{C} so that node 0 is decoupled from all other nodes in $\hat{\mathbf{C}}^{decoupling}$ (see Figure 8b). Figure 8a shows the behavior of the system as node 0 desynchronizes following step 600, the point at which the underlying structure is changed.

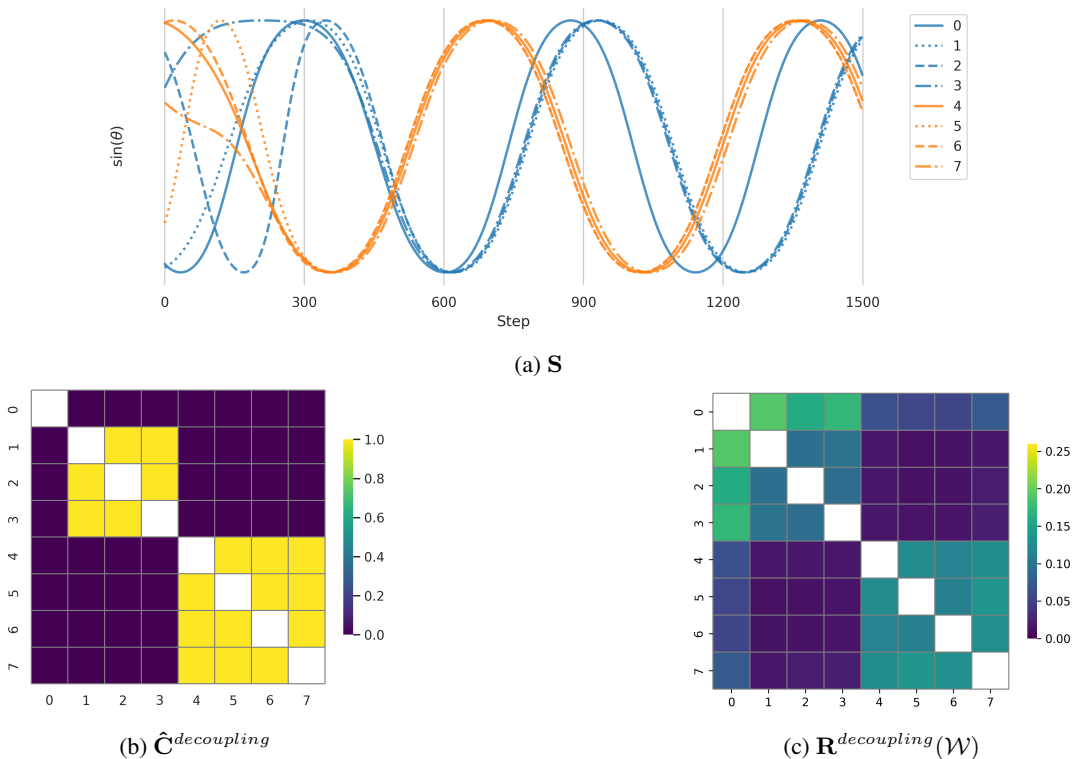


Figure 8: Case 1 - Decoupling. Signals (a), shuffled coupling matrix (b) and average observation adjacency matrix for \mathcal{W} with start steps 600-1200 (c).

Inspection of the health state adjacency in Figure 8c shows that connections involving node 0 which had been removed in $\hat{\mathbf{C}}^{decoupling}$ are highlighted.

5.3.5 Case 2 - Swap

For our second test case we consider a system in which two components swap the subsystem to which they belong. We adjust \mathbf{C} so that node 0 and node 7 become coupled to the opposite set of oscillators in $\hat{\mathbf{C}}^{swap}$ (Figure 9b).

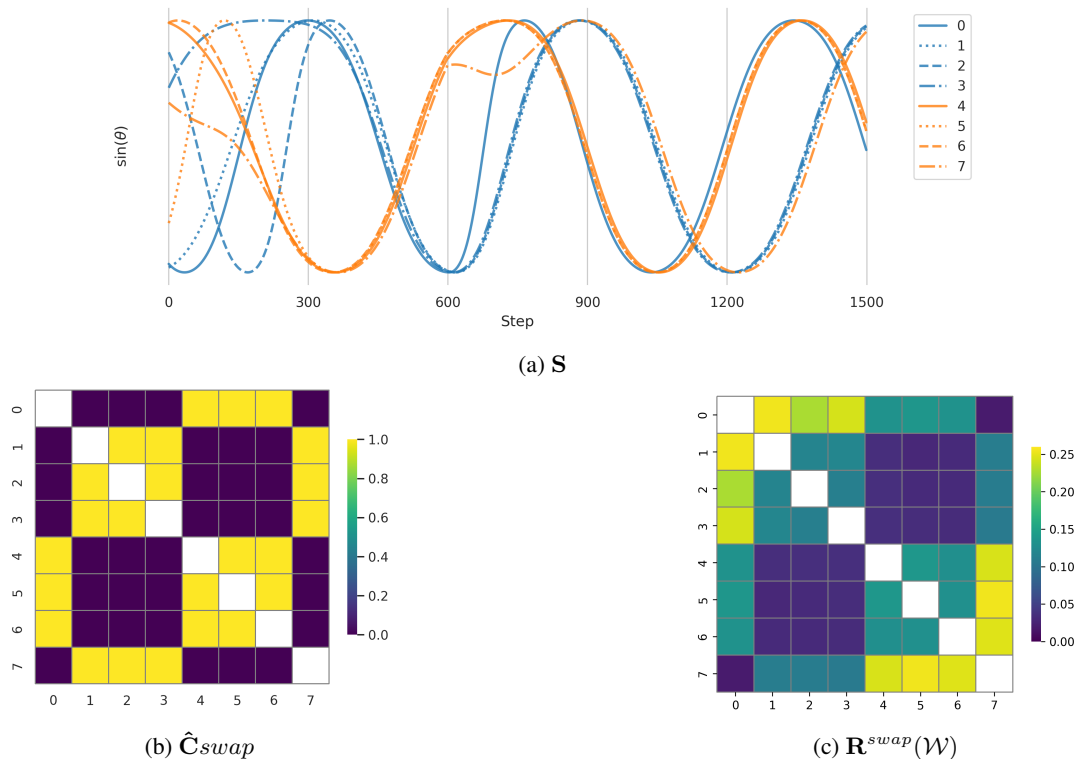


Figure 9: Case 2 - Swap. Signals (a), shuffled coupling matrix (b) and average observation adjacency matrix for \mathcal{W} with start steps 600-1200 (c).

Figure 9a shows the behavior of the system as nodes 0 and 7 synchronize to nodes 4-6 and nodes 1-3, respectively, following step 600. Inspection of the health state adjacency in Figure 9c shows that indeed all connections involving node 0 or node 7 are highlighted.

5.4 Link to Component-centric Methods

While we consider a diagnosis to be a set of faulty edges, our method can also be linked back to health states of components. We can sum entries in \mathbf{R}_t per component and apply the normalized exponential function to answer the question: "What is the probability that a component is faulty?"

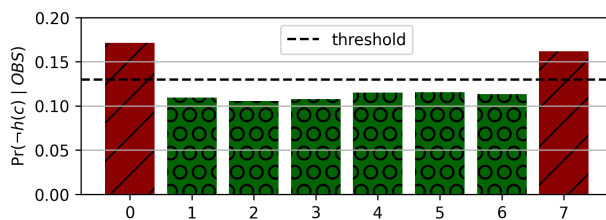


Figure 10: Probability of nodes being faulty for the swap case.

Figure 10 shows such probabilities for Case 2. Using a threshold we get a set of faulty components. The selection of a suitable threshold is considered a separate task which can be solved algorithmically or left to the operator.

6 Conclusion

In this paper, we have introduced a novel data-driven framework that successfully combines traditional model-based diagnosis concepts with deep graph structure learning to diagnose faults. Our approach is unique in its emphasis on

learning a graph structural model of the system from data. By addressing our three primary research questions, we have demonstrated the potential of a machine learning-based method to replace manual, expertise-demanding model construction in system diagnosis.

Firstly, we have shown that it is feasible to learn a system representation in the form of an adjacency matrix directly from data. Our method takes advantage of the rich temporal structure inherent in the data, thereby sidestepping the need for laborious manual system modeling.

Secondly, our model design dynamically generates observations from multivariate time-series data. This reflects the evolving state of the system under observation and enables a dynamic, responsive element in our diagnostic approach.

Thirdly, we have validated that residuals can be directly inferred from the learned reference and observation adjacency matrices. This represents a paradigm shift from traditional model-based diagnostic systems and expands the possibilities of the diagnostic process.

However, a potential limitation of our approach is that it heavily relies on the quality and relevance of the data fed into the system. Therefore, while the graph-centric approach provides a powerful tool for fault diagnosis, its effectiveness is closely tied to the quality of the input data.

While our findings are encouraging, our approach needs to be validated further on a wider variety of datasets, system types and real-world scenarios. Future work might involve refining the graph generation process, incorporating domain knowledge or exploring the generalizability of this approach to other domains.

Acknowledgments

This research has been conducted as part of the project SmartShip which is funded by dtec.bw – Digitalization and Technology Research Center of the Bundeswehr. dtec.bw is funded by the European Union – NextGenerationEU.

References

- [1] Louise Travé-Massuyès and Teresa Escobet. Bridge: Matching model-based diagnosis from fdi and dx perspectives. *Fault Diagnosis of Dynamic Systems: Quantitative and Qualitative Approaches*, pages 153–175, 2019.
- [2] Johan De Kleer and Brian C Williams. Diagnosing multiple faults. *Artificial intelligence*, 32(1):97–130, 1987.
- [3] Raymond Reiter. A theory of diagnosis from first principles. *Artificial intelligence*, 32(1):57–95, 1987.
- [4] Peter Struss and Chris Price. Model-based systems in the automotive industry. *AI magazine*, 24(4):17–17, 2003.
- [5] Brian C Williams, P Pandurang Nayak, et al. A model-based approach to reactive self-configuring systems. In *Proceedings of the national conference on artificial intelligence*, pages 971–978, 1996.
- [6] Eliahu Khalastchi, Meir Kalech, and Lior Rokach. Sensor fault detection and diagnosis for autonomous systems. In *Proceedings of the 2013 international conference on Autonomous agents and multi-agent systems*, pages 15–22, 2013.
- [7] Rui Abreu, Peter Zoetewij, and Arjan JC Van Gemund. Simultaneous debugging of software faults. *Journal of Systems and Software*, 84(4):573–586, 2011.
- [8] Alexander Diedrich and Oliver Niggemann. On residual-based diagnosis of physical systems. *Engineering Applications of Artificial Intelligence*, 109:104636, 2022.
- [9] Brian C Williams and Robert J Ragno. Conflict-directed a* and its role in model-based embedded systems. *Discrete Applied Mathematics*, 155(12):1562–1595, 2007.
- [10] Roni Stern, Meir Kalech, Alexander Feldman, and Gregory Provan. Exploring the duality in conflict-directed model-based diagnosis. In *Proceedings of the AAAI Conference on Artificial Intelligence*, volume 26, pages 828–834, 2012.
- [11] Mogens Blanke, Michel Kinnaert, Jan Lunze, Marcel Staroswiecki, and Jochen Schröder. *Diagnosis and fault-tolerant control*, volume 2. Springer, 2006.
- [12] Janos Gertler. *Fault detection and diagnosis in engineering systems*. CRC press, 1998.
- [13] Dilek Düştegör, Erik Frisk, Vincent Cocquempot, Mattias Krysander, and Marcel Staroswiecki. Structural analysis of fault isolability in the damadics benchmark. *Control Engineering Practice*, 14(6):597–608, 2006.
- [14] Erik Frisk, Mattias Krysander, and Teresa Escobet. Structural analysis. *Fault Diagnosis of Dynamic Systems: Quantitative and Qualitative Approaches*, pages 43–68, 2019.

- [15] Mattias Krysanter and Erik Frisk. Sensor placement for fault diagnosis. *IEEE Transactions on Systems, Man, and Cybernetics-Part A: Systems and Humans*, 38(6):1398–1410, 2008.
- [16] Zonghan Wu, Shirui Pan, Fengwen Chen, Guodong Long, Chengqi Zhang, and S Yu Philip. A comprehensive survey on graph neural networks. *IEEE transactions on neural networks and learning systems*, 32(1):4–24, 2020.
- [17] Michael M Bronstein, Joan Bruna, Taco Cohen, and Petar Veličković. Geometric deep learning: Grids, groups, graphs, geodesics, and gauges. *arXiv preprint arXiv:2104.13478*, 2021.
- [18] Franco Scarselli, Marco Gori, Ah Chung Tsoi, Markus Hagenbuchner, and Gabriele Monfardini. The graph neural network model. *IEEE transactions on neural networks*, 20(1):61–80, 2008.
- [19] Joan Bruna, Wojciech Zaremba, Arthur Szlam, and Yann LeCun. Spectral networks and locally connected networks on graphs. *arXiv preprint arXiv:1312.6203*, 2013.
- [20] Thomas N Kipf and Max Welling. Semi-supervised classification with graph convolutional networks. *arXiv preprint arXiv:1609.02907*, 2016.
- [21] David K Duvenaud, Dougal Maclaurin, Jorge Iparraguirre, Rafael Bombarell, Timothy Hirzel, Alán Aspuru-Guzik, and Ryan P Adams. Convolutional networks on graphs for learning molecular fingerprints. *Advances in neural information processing systems*, 28, 2015.
- [22] Bing Yu, Haoteng Yin, and Zhanxing Zhu. Spatio-temporal graph convolutional networks: A deep learning framework for traffic forecasting. *arXiv preprint arXiv:1709.04875*, 2017.
- [23] Weiqi Chen, Ling Chen, Yu Xie, Wei Cao, Yusong Gao, and Xiaojie Feng. Multi-range attentive bicomponent graph convolutional network for traffic forecasting. In *Proceedings of the AAAI conference on artificial intelligence*, volume 34, pages 3529–3536, 2020.
- [24] Shiwen Wu, Fei Sun, Wentao Zhang, Xu Xie, and Bin Cui. Graph neural networks in recommender systems: A survey. *ACM Comput. Surv.*, 55(5):1–37, December 2022.
- [25] Michael Schlichtkrull, Thomas N Kipf, Peter Bloem, Rianne van den Berg, Ivan Titov, and Max Welling. Modeling relational data with graph convolutional networks. In *The Semantic Web*, pages 593–607. Springer International Publishing, 2018.
- [26] Yanqiao Zhu, Weizhi Xu, Jinghao Zhang, Yuanqi Du, Jieyu Zhang, Qiang Liu, Carl Yang, and Shu Wu. A survey on graph structure learning: Progress and opportunities. *arXiv preprint arXiv:2103.03036*, 2021.
- [27] Luca Franceschi, Mathias Niepert, Massimiliano Pontil, and Xiao He. Learning discrete structures for graph neural networks. In *International conference on machine learning*, pages 1972–1982. PMLR, 2019.
- [28] Donghan Yu, Ruohong Zhang, Zhengbao Jiang, Yuexin Wu, and Yiming Yang. Graph-revised convolutional network. In *Machine Learning and Knowledge Discovery in Databases: European Conference, ECML PKDD 2020, Ghent, Belgium, September 14–18, 2020, Proceedings, Part III*, pages 378–393. Springer, 2021.
- [29] Wei Jin, Yao Ma, Xiaorui Liu, Xianfeng Tang, Suhang Wang, and Jiliang Tang. Graph structure learning for robust graph neural networks. In *Proceedings of the 26th ACM SIGKDD international conference on knowledge discovery & data mining*, pages 66–74, 2020.
- [30] Ruijia Wang, Shuai Mou, Xiao Wang, Wanpeng Xiao, Qi Ju, Chuan Shi, and Xing Xie. Graph structure estimation neural networks. In *Proceedings of the Web Conference 2021*, pages 342–353, 2021.
- [31] Yu Chen, Lingfei Wu, and Mohammed Zaki. Iterative deep graph learning for graph neural networks: Better and robust node embeddings. *Advances in neural information processing systems*, 33:19314–19326, 2020.
- [32] Bahare Fatemi, Layla El Asri, and Seyed Mehran Kazemi. Slaps: Self-supervision improves structure learning for graph neural networks. *Advances in Neural Information Processing Systems*, 34:22667–22681, 2021.
- [33] Benedek Rozemberczki, Paul Scherer, Yixuan He, George Panagopoulos, Alexander Riedel, Maria Astefanoaei, Oliver Kiss, Ferenc Beres, Guzmán López, Nicolas Collignon, and Rik Sarkar. Pytorch geometric temporal: Spatiotemporal signal processing with neural machine learning models, 2021.
- [34] Jiong Zhu, Yujun Yan, Lingxiao Zhao, Mark Heimann, Leman Akoglu, and Danai Koutra. Beyond homophily in graph neural networks: Current limitations and effective designs. *Advances in Neural Information Processing Systems*, 33:7793–7804, 2020.
- [35] Shaojie Bai, J Zico Kolter, and Vladlen Koltun. An empirical evaluation of generic convolutional and recurrent networks for sequence modeling. *arXiv preprint arXiv:1803.01271*, 2018.
- [36] Keyulu Xu, Weihua Hu, Jure Leskovec, and Stefanie Jegelka. How powerful are graph neural networks? *arXiv preprint arXiv:1810.00826*, 2018.

- [37] Yoshiki Kuramoto. Self-entrainment of a population of coupled non-linear oscillators. In *International Symposium on Mathematical Problems in Theoretical Physics*, pages 420–422. Springer Berlin Heidelberg, 1975.
- [38] Adam Paszke, Sam Gross, Francisco Massa, Adam Lerer, James Bradbury, Gregory Chanan, Trevor Killeen, Zeming Lin, Natalia Gimelshein, Luca Antiga, et al. Pytorch: An imperative style, high-performance deep learning library. *Advances in neural information processing systems*, 32, 2019.
- [39] Fabrizio Damicelli. Python implementation of the kuramoto model. <https://github.com/fabridamicelli/kuramoto>, 2019.
- [40] Diederik P Kingma and Jimmy Ba. Adam: A method for stochastic optimization. *arXiv preprint arXiv:1412.6980*, 2014.